Relationships between Structural Parameters and Raman Frequencies for Some Planar and Nonplanar Nickel(II) Porphyrins

J. A. Shelnutt,*,†,‡ C. J. Medforth,§ M. D. Berber,§ K. M. Barkigia,⊥ and K. M. Smith*,§

Contribution from the Fuel Science Division 6211, Sandia National Laboratories, Albuquerque, New Mexico 87185, Department of Chemistry, University of New Mexico, Albuquerque, New Mexico 87131, Department of Chemistry, University of California, Davis, California 95616, and Department of Applied Science, Brookhaven National Laboratory, Upton, New York 11973. Received October 18, 1990

Abstract: Molecular mechanics calculations, based on a force field derived from a previously published normal coordinate analysis for NiOEP (1) and the X-ray structure of NiOEP B triclinic form, have been used to predict the structures of NiTPP (2), NiP (3), and several recently synthesized nickel porphyrins which bear alkyl or phenyl groups at all 12 peripheral positions (4–10). These calculations predict that porphyrins 4 (NiOMTPP), 5 (NiOETPP), 6 (NiOPTPP), 7 (NiDPP), 9 (NiTC₆TPP), and 10 (NiTC₇TPP) adopt a saddle conformation with varying degrees of nonplanarity of the macrocycle. To evaluate the accuracy of these calculations, a single-crystal X-ray structure of the porphyrin with the most nonplanar calculated structure (NiOPTPP) was determined. The agreement between observed and calculated structures is good, both in terms of the general molecular conformation and more subtle structural differences such as a decrease in core size and increase in the C_aNC_a bond angle compared to planar nickel porphyrins. The structural parameters obtained from these calculations were then used to investigate the relationship between core size and the frequency of the structure-sensitive Raman lines (ν_4, ν_3, ν_2, and ν_{19}). The linear relationship between core size and Raman frequency has a positive slope, in contrast to the negative slope exhibited by the usual core size–Raman frequency relationship. Thus, it is not the core size that determines the frequencies of the structure-sensitive Raman lines. On the other hand, the linear correlation between the C_aNC_a angle and Raman frequency has a negative slope for both the nickel porphyrins used in this study and the metalloporphyrins of the conventional core-size relationship, suggesting a more direct relationship between this angle and the marker line frequencies.

Introduction

The importance of nonplanar macrocyclic conformations in the biochemical function of tetrapyrroles in proteins has recently been recognized.[1,2] Domed porphyrin macrocycles have been observed in the X-ray crystal structures of heme proteins,[3–5] and nonplanar macrocycles are found in the crystal structure of the bacterial photosynthetic reaction center.[6–8] In the latter case, twisting of the pyrrole rings by as much as 17° is observed for several of the tetrapyrroles, including the bacteriochlorophylls of the special pair.[8] Functional significance has been attached to nonplanar tetrapyrrole conformations in the case of vitamin B₁₂ and B₁₂-dependent enzymes,[9] photosynthetic reaction centers,[10] and methylreductase.[11] Methylreductase contains cofactor F₄₃₀, a nickel(II)-corphin derivative, which has all four pyrrole rings and two of the four bridging meso carbon atoms reduced.[12] Related nickel corphinates exhibit some of the most nonplanar tetrapyrrole structures known.[13,14] In the cases of both F₄₃₀ and B₁₂, it is thought that the degree of planarity of the macrocycle can modulate axial ligation at the metal. The protein environment might also exert influence over the planarity of the macrocycle and, in this way, modulate ligand affinity and other properties.[10] In the case of ligand affinity, evidence for this mechanism has been found recently in studies of nickel-reconstituted hemoglobin and myoglobin.[15–21]

Spectroscopic probes of macrocycle planarity are needed to aid in evaluating the importance of nonplanar structures in the function of proteins. In this regard, resonance Raman spectroscopy has been particularly successful in detecting and quantifying the nonplanarity of nickel porphyrins in various environments[19–21] and in evaluating the effects of the porphyrin's environment upon the planarity of the macrocycle.[21] Previously, we showed that several nickel porphyrins in solution exist as an equilibrium mixture of both planar and ruffled conformers.[19,21] The two conformers exhibit different frequencies for the structure-sensitive Raman

lines. The two forms were identified in nickel octaethylporphyrin (NiOEP) solutions by showing that the Raman frequencies for the components of the structure-sensitive lines agree with the frequencies observed for the corresponding single crystals composed of either planar or ruffled NiOEP.[20] Subsequently, we observed

(1) Horning, T. L.; Fujita, E.; Fajer, J. *J. Am. Chem. Soc.* **1986**, *108*, 323.
(2) Eschenmoser, A. *Ann. N.Y. Acad. Sci.* **1986**, *471*, 108.
(3) Takano, T. *J. Mol. Biol.* **1977**, *110*, 537.
(4) Deatherage, J. F.; Loe, R. S.; Anderson, C. M.; Moffat, K. *J. Mol. Biol.* **1976**, *104*, 687.
(5) Ladner, R. C.; Heidner, E. J.; Perutz, M. F. *J. Mol. Biol.* **1977**, *114*, 385.
(6) Deisenhofer, J.; Epp, O.; Miki, K.; Huber, R.; Michel, H. *Nature* **1985**, *318*, 618.
(7) (a) Deisenhofer, J.; Epp, O.; Miki, K.; Huber, R.; Michel, H. *J. Mol. Biol.* **1984**, *180*, 385. (b) Zinth, W.; Knapp, E. W.; Fischer, S. F.; Kaiser, W.; Deisenhofer, J.; Michel, W. *Chem. Phys. Lett.* **1985**, *119*, 1.
(8) Protein Data Bank, Brookhaven National Laboratories, Upton, NY.
(9) Geno, M. K.; Halpern, J. *J. Am. Chem. Soc.* **1987**, *109*, 1238.
(10) Barkigia, K. M.; Chantranupong, L.; Smith, K. M.; Fajer, J. *J. Am. Chem. Soc.* **1988**, *110*, 7566.
(11) (a) Furenlid, L. R.; Renner, M. W.; Smith, K. M.; Fajer, J. *J. Am. Chem. Soc.* **1990**, *112*, 1634. (b) Furenlid, L. R.; Renner, M. W.; Fajer, J. *J. Am. Chem. Soc.* **1990**, *112*, 8987.
(12) Pfaltz, A.; Jaun, B.; Fässler, A.; Eschenmoser, A.; Jaenchen, R.; Gilles, H. H.; Diekert, G.; Thauer, R. K. *Helv. Chim. Acta* **1982**, *65*, 828.
(13) Kratky, C.; Waditschatka, R.; Angst, C.; Johansen, J. E.; Plaquerent, J. C.; Schreiber, J.; Eschenmoser, A. *Helv. Chim. Acta* **1985**, *68*, 1312.
(14) Waditschatka, R.; Kratky, C.; Juan, B.; Heinzer, J.; Eschenmoser, A. *J. Chem. Soc., Chem. Commun.* **1985**, 1604.
(15) Shelnutt, J. A.; Alston, K.; Ho, J.-Y.; Yu, N.-T.; Yamamoto, T.; Rifkind, J. M. *Biochemistry* **1986**, *25*, 620.
(16) Findsen, E. W.; Alston, K.; Shelnutt, J. A.; Ondrias, M. R. *J. Am. Chem. Soc.* **1986**, *108*, 4009.
(17) Shelnutt, J. A.; Alston, K.; Findsen, E. W.; Ondrias, M. R.; Rifkind, J. M. In *Porphyrins: Excited States and Dynamics*; Gouterman, M., Rentzepis, P. M., Straub, K. D., Eds.; ACS Symp. Series 321; American Chemical Society: Washington, DC, 1986; Chapter 16.
(18) Shelnutt, J. A.; Findsen, E. W.; Ondrias, M. R.; Alston, K. In *Metal Complexes in Fossil Fuels*; Filby, R. H., Branthaver, J. F., Eds.; ACS Symp. Series 344; American Chemical Society: Washington, DC, 1987; Chapter 24.
(19) Alden, R. G.; Crawford, B. A.; Doolen, R.; Ondrias, M. R.; Shelnutt, J. A. *J. Am. Chem. Soc.* **1989**, *111*, 2070.
(20) Brennan, T. D.; Scheidt, W. R.; Shelnutt, J. A. *J. Am. Chem. Soc.* **1988**, *110*, 3919.
(21) Alden, R. G.; Ondrias, M. R.; Shelnutt, J. A. *J. Am. Chem. Soc.* **1990**, *112*, 691.

* To whom correspondence should be addressed.
† Sandia National Laboratories.
‡ University of New Mexico.
§ University of California.
⊥ Brookhaven National Laboratory.

4078 *J. Am. Chem. Soc., Vol. 113, No. 11, 1991*

Shelnutt et al.

the influence of complex formation, dimerization, and protein binding upon the equilibrium between planar and ruffled conformers.[21,22] For example, binding of Ni protoporphyrin IX (NiProtoP) to the active site of hemoglobin results in a planar macrocycle at the four-coordinate sites in the protein.[21] That is, protein binding of NiProtoP shifts the equilibrium overwhelmingly in favor of the planar conformer. By way of contrast, the isolated α-subunits of hemoglobin allow some ruffling of NiProtoP to occur in the active site. These differences in macrocycle conformation account for the differences in affinity of Ni(II) for the proximal histidine observed for the two proteins. In these studies we used the size of the shifts in a group of structure-sensitive lines as a measure of the degree of nonplanarity of the porphyrin macrocycle.

Correlations between various structural parameters of the macrocycle and vibrational frequencies are of prevailing importance in resonance Raman studies of tetrapyrrole-containing proteins and other chemical and photochemical reactions mediated by tetrapyrroles.[23,24] For metalloporphyrins, correlations between Raman line frequencies and metal core size,[25-27] oxidation state of the central metal[28] and the porphyrin ring,[29,30] spin state,[31] coordination number,[32] and properties of the axial ligand[33] are examples. One of the most significant and useful structural relationships is that between core size and the frequencies of a group of lines between 1300 and 1500 cm^{-1} dubbed the core-size marker lines. The Raman core-size marker lines provide a remarkably reliable structural correlation that has been used to advantage in many structure-function investigations of tetrapyrrole-containing proteins and in studies of metalloporphyrins in other chemical environments.

Application of the core-size marker correlation has been confounded of late because the lines are also sensitive to macrocycle planarity. In fact, in the inceptive work by Spaulding et al.,[25] the authors noted that the frequencies for the nonplanar, ruffled crystal structure of NiOEP did not fall on the linear relationship observed for other metalloporphyrins. An attempt has been made to incorporate planarity into the relationship between structure and core-size marker line frequencies[34] but with limited success. Recently, the problem of the dual dependence on planarity *and* core size has become more acute since the core-size markers are now being applied to porphyrin cations and reduced tetrapyrrole macrocycles like chlorins, chlorophylls, and corphinates,[35,36] where the lower aromaticity of the reduced tetrapyrroles compared with porphyrins makes the occurrence of nonplanar conformers more likely.

In the present work, we investigate the structures of a series of porphyrins with varying degrees of nonplanarity caused by steric interactions among substituent groups attached at the periphery of the macrocycle. The nickel(II) octaalkyl(aryl)tetraphenylporphyrin (NiOATPP) series consists of octamethyltetraphenylporphyrin **4** (NiOMTPP), octaethyltetraphenylporphyrin

5 (NiOETPP), octapropyltetraphenylporphyrin **6** (NiOPTPP), tetracyclopentenyltetraphenylporphyrin **8** (NiTC₅TPP), tetra-
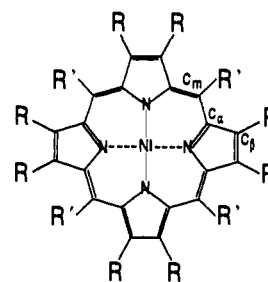
1 NiOEP, R = ethyl; R' = H
2 NiTPP, R = H; R' = phenyl
3 NiP, R = R' = H
4 NiOMTPP, R = methyl; R' = phenyl
5 NiOETPP, R = ethyl; R' = phenyl
6 NiOPTPP, R = propyl; R' = phenyl
7 NiDPP, R = R' = phenyl
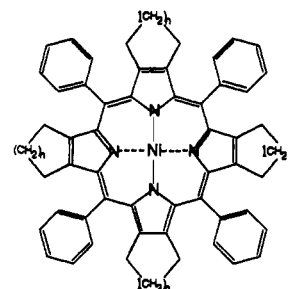
8 NiTC₅TPP, $n = 1$
9 NiTC₆TPP, $n = 2$
10 NiTC₇TPP, $n = 3$

cyclohexenyltetraphenylporphyin **9** (NiTC₆TPP), tetracycloheptenyltetraphenylporphyrin **10** (NiTC₇TPP), and dodecaphenylporphyrin **7** (NiDPP). Nickel porphine **3** (NiP), nickel octaethylporphyrin **1** (NiOEP), and nickel tetraphenylporphyrin **2** (NiTPP) were included with the NiOATPPs for comparison purposes. Existing X-ray crystallographic structural studies of NiOEP[20,37] have been augmented by structures of the other porphyrins in the NiOATPP series that we have obtained from energy-optimization calculations by using a classical force field based on a recent NiOEP normal coordinate analysis.[38] We have also determined the crystal structure of NiOPTPP,[39] which is predicted to have the most ruffled macrocycle of all of the NiOATPPs based on the energy-optimized structures, and there is good agreement between the calculated and X-ray crystal structures.

By using the structural parameters obtained from these molecular mechanics calculations and the X-ray structure of NiOPTPP, we have investigated correlations between the Raman frequencies of structure-sensitive lines and factors such as nonplanarity, core size, and the $C_{\alpha}NC_{\alpha}$ angle. Finally, we have investigated the visible absorption spectra of these nonplanar porphyrins in a range of coordinating and noncoordinating solvents to illustrate the influence of nonplanarity on the chemical and photophysical properties of the macrocycle.

Materials and Methods

Molecular Mechanics Calculations. Energy-optimized porphyrin structures were determined with BIOGRAF software (BioDesign, Inc.) by using a conjugate-gradient minimization technique with a force field that we defined based on a normal coordinate analysis of NiOEP[38] and

(22) Crawford, B. A.; Ondrlas, M. R.; Shelnutt, J. A. *J. Phys. Chem.* **1990**, *94*, 6647.

(23) Spiro, T. G. In *Iron Porphyrins*; Lever, A. B. P., Gray, H. B., Eds.; Addison-Wesley: Reading, 1983; Chapter 3.

(24) Felton, R. H.; Yu, N.-T. In *The Porphyrins*; Dolphin, D., Ed.; Academic: New York, 1978; Vol. 3, Chapter 8.

(25) Spaulding, L. D.; Chang, C. C.; Yu, N.-T.; Felton, R. H. *J. Am. Chem. Soc.* **1975**, *97*, 2517.

(26) Stong, J. D.; Spiro, T. G.; Kubaska, R. J.; Shupack, S. I. *J. Raman Spectrosc.* **1980**, *9*, 312.

(27) Parthasarathi, N.; Hansen, C.; Yamaguchi, S.; Spiro, T. G. *J. Am. Chem. Soc.* **1987**, *109*, 3865.

(28) Yamamoto, T.; Palmer, G.; Gill, D.; Salmeen, I. T.; Rimai, L. *J. Biol. Chem.* **1973**, *248*, 5211.

(29) Ksenofontova, N. M.; Maslov, V. G.; Sidorov, A. N.; Bobovich, Ya. S. *Opt. Spectrosc. (Engl. Transl.)* **1976**, *40*, 462.

(30) Yamaguchi, H.; Nakano, M.; Itoh, K. *Chem. Lett.* **1982**, 1397.

(31) Spiro, T. G. In *Chemical and Biochemical Applications of Lasers*; Moore, C. B., Ed.; Academic: New York, 1974; Chapter 2.

(32) Teraoka, J.; Kitagawa, T. *J. Phys. chem.* **1980**, *84*, 1928.

(33) Spiro, T. G.; Burke, J. M. *J. Am. Chem. Soc.* **1976**, *98*, 5482.

(34) Spiro, T. G.; Stong, J. D.; Stein, P. *J. Am. Chem. Soc.* **1979**, *101*, 2648.

(35) Andersson, L. A.; Loehr, T. M.; Sotiriou, C.; Wu, W.; Chang, C. K. *J. Am. Chem. Soc.* **1986**, *108*, 2908.

(36) Shelnutt, J. A. *J. Am. Chem. Soc.* **1987**, *109*, 4169.

(37) Cullen, D. L.; Meyer, E. F., Jr. *J. Am. Chem. Soc.* **1974**, *96*, 2095.

(38) (a) Abe, M.; Kitagawa, T.; Kyogoku, Y. *J. Chem. Phys.* **1978**, *69*, 4526. (b) Li, X.-Y.; Czernuszewicz, R. S.; Kincaid, J. R.; Spiro, T. G. *J. Am. Chem. Soc.* **1989**, *111*, 7012. (c) Li, X.-Y.; Czernuszewicz, R. S.; Kincaid, J. R.; Stein, P.; Spiro, T. G. *J. Phys. Chem.* **1990**, *94*, 47.

(39) Barkigia, K. M.; Fajer, J.; Medforth, C. J.; Smith, K. M., manuscript in preparation.

the DREIDING force field.[40]　The energy is calculated from the equation

$$E = E_b + E_\theta + E_\phi + E_\omega + E_{nb}$$

where E_b is the bond stretching contribution to the internal energy

$$E_b = \sum \tfrac{1}{2} K_r (r - r_0)^2$$

with the unconstrained bond distance r_0 and force constant K_r in kcal/mol-Å², and the sum is over all bonds of the molecule. Similarly, E_θ is the bond bending contribution

$$E_\theta = \sum \tfrac{1}{2} H_\theta (\theta - \theta_0)^2$$

with θ_0 as the unconstrained bond angle and H_θ as the bending force constant (in kcal/mol-rad²). E_ϕ is the torsion energy for two bonds connected by a common bond

$$E_\phi = \sum \tfrac{1}{2} \tau_\phi (1 - d \cos n\phi)$$

where τ_ϕ is one-half the rotational barrier in kcal/mol, n is the periodicity of the potential function, and d is a phase factor (= +1 or −1). E_ω is the inversion or improper torsion terms,[41] which act to maintain the planarity ($\omega_0 = 0$) of aromatic ring systems

$$E_\omega = \sum \tfrac{1}{2} \gamma_\omega (\omega - \omega_0)^2$$

and E_{nb} is the van der Waals contribution given by

$$E_{nb} = \sum_i \sum_j (D_i D_j)^{1/2} \{ -2[(R_i + R_j)/r_{ij}]^6 + [(R_i + R_j)/r_{ij}]^{12} \}$$

where D_i (D_{nb} in Table II, see supplementary material) is the depth of the Lennard–Jones potential well, R_i is the van der Waals radius of the ith atom (R_{nb} in Table II), and r_{ij} is the distance between the ith and jth atoms. A cutoff distance of 9 Å and a switching function[40,41] was used for the van der Waals potential energy term. Interactions between bonded atoms and atoms involved in angle interactions were neglected.

Electrostatic potential energy terms also were evaluated and were found to have only a small effect on the structure. The structures reported do not include the effects of partial charges on the atoms. Table I of the supplementary material gives the force field parameters used for the internal coordinates of the molecule. The interaction force constants determined in the normal coordinate analysis were ignored for the calculation of the energy optimized structures. Table II of the supplementary material gives the nonbonding force field parameters.

The calculations were carried out on a MicroVAX II computer (Digital Equipment Corp.) and displayed on a PS390 graphics workstation (Evans & Sutherland, Inc.).

Synthesis of Nickel Octaalkyl(aryl)tetraphenylporphyrins and X-ray Structure Determinations. With the exception of OPTPP, syntheses of the OATPPs used in this study have been reported previously.[42–44] OPTPP was prepared by using the same general procedure. Benzaldehyde and 3,4-dipropylpyrrole were condensed in the presence of a catalytic amount of BF_3–OEt_2 to form the porphyrinogen, which was then oxidized to the required porphyrin using 2,3-dichloro-5,6-dicyano-1,4-benzoquinone (DDQ). The porphyrin was purified by using a Brockmann grade III alumina column, eluting first with 1% methanol in dichloromethane to remove fast running pigments and then with 4% methanol in dichloromethane to obtain the porphyrin. Visible absorption and proton NMR spectra of the porphyrin fraction showed that a mixture of the porphyrin free base and dication was present. Crystals of the free base porphyrin were obtained by dissolving the mixture in dichloromethane and adding a 1% solution of KOH in ethanol. The yield of OPTPP was 25%.

Nickel porphyrins were prepared by using the acetate method.[45] The general procedure was as follows. Porphyrin (10–50 mg depending upon availability) was dissolved in chloroform (25 mL) and brought to reflux, whereupon a saturated solution of nickel acetate in 95% methanol/5% acetic acid (1 mL) was added, and the mixture was shielded from ambient light and refluxed under nitrogen. The rate at which metalation occurred was found to vary widely, from complete metalation in less than 30 min for TC_6TPP to incomplete metalation after several days for DPP.

In the case of TC_5TPP, the nickel complex precipitated out of the reaction mixture and was filtered off.[46] When metalation was incomplete, the nickel porphyrin was separated by using a Brockmann grade III alumina column and appropriate solvent system. The nickel porphyrins were recrystallized by adding methanol to a solution of the porphyrin in dichloromethane, except for $NiTC_5TPP$ which was only sparingly soluble. Crystals of NiOPTPP suitable for X-ray structure determination were grown by slow diffusion of methanol into a solution of the porphyrin in dichloromethane.

The X-ray structure of NiOPTPP was obtained at room temperature and at 200 K.[39] As the temperature was lowered, the crystal underwent a phase transition which allowed us to study the molecule in two different crystalline environments. Final values for the refinement factors, R_F and R_{wF}, are 0.053 and 0.055 at room temperature and 0.054 and 0.060 at 200 K. Differences between the conformations of the porphyrins in the two NiOPTPP structures were small. The full structures will be reported elsewhere.[39] Preliminary X-ray structures of NiOETPP and $NiTC_6TPP$ show a nonplanar conformation similar to that of NiOPTPP.[47] An EXAFS study of $NiTC_5TPP$ is also currently in progress to determine the Ni–N distance in this compound.[48]

Resonance Raman and UV–Visible Absorption Spectroscopies. Solution samples for Raman spectra were prepared by dissolving the nickel porphyrins in neat carbon disulfide or dichloromethane at between 1 × 10^{-5} and 1 × 10^{-4} M concentrations. Solvents were of the highest purity available commercially. To each compartment of the Raman cell were added 100–200 µL of the porphyrin solutions. For the polarized Raman spectra, aliquots from the same porphyrin solution were added to each compartment. For comparisons between different NiOATPPs, two different solutions were added to the two compartments. Usually NiOETPP was added to the reference chamber, since this compound was more plentiful.

The resonance Raman spectra of pairs of NiOATPPs were obtained on a dual-channel Raman spectrometer described previously.[49] This Raman difference spectrometer allows accurate comparisons of two samples, capable of giving frequency differences to at least 0.1 cm⁻¹ accuracy for Raman lines that have good signal-to-noise characteristics. For the spectra reported here, frequency differences were obtained from the peak positions of the lines in the fast Fourier-transform smoothed spectra obtained in pairs. Frequency differences of corresponding lines of the two samples obtained in this fashion typically are accurate to better than ±0.4 cm⁻¹, twice the 0.2-cm⁻¹ grating increment used in scanning the spectrometer, and are adequate for the present purposes.

The 457.9-nm line of an argon ion laser or the 413.1-nm line of a krypton ion laser were used to excite the Raman spectra. The 457.9-nm laser line is to the red of the Soret absorption band for most of the NiOATPPs but close enough to the absorption maximum to provide strong resonance enhancement of the porphyrin vibrational modes. The 413.1-nm line is to the blue of the Soret band for most members of the NiOATPP series. The slits of the spectrometer were adjusted to give 3–4-cm⁻¹ resolution.

The partitoned Raman cell was rotated at 50 Hz to prevent sample heating. No porphyrin decomposition was noted during the (typically) 5–15 half-hour scans of the spectrum. Sample decomposition was monitored by UV–visible spectroscopy before and after obtaining the Raman spectrum in some cases and by examination of selected half-hour scans of the Raman spectrum obtained during signal averaging.

For the polarized spectra, a polaroid sheet was attached to the cylindrical face of the Raman cell and rotated with the cell. The polaroid attached to one side of the cell was oriented parallel to the incident laser polarization and was perpendicular to the incident polarization on the other side of the cell. Thus, both parallel and perpendicular polarized spectra were obtained simultaneously in a 90° scattering geometry.

Raman spectra were obtained from powders or single crystals of many of the nickel porphyrins, and frequencies of the structure-sensitive Raman

(40) Mayo, S. L.; Olafson, B. D.; Goddard III, W. A. *J. Phys. Chem.* **1990**, *94*, 8897.

(41) Brooks, B. R.; Bruccoleri, R. E.; Olafson, B. D.; States D. J.; Swaminathan, S.; Karplus, M. *J. Comput. Chem.* **1983**, *4*, 187.

(42) Medforth, C. J.; Berber, M. D.; Smith, K. M.; Shelnutt, J. A. *Tetrahedron Lett.* **1990**, *31*, 3719.

(43) Barkigia, K. M.; Berber, M. D.; Fajer, J.; Medforth, C. J.; Renner, M. W.; Smith, K. M. *J. Am. Chem. Soc.* **1990**, *112*, 8851.

(44) Medforth, C. J.; Smith, K. M. *Tetrahedron Lett.* **1990**, *31*, 5583.

(45) *Porphyrins and Metalloporphyrins*; Smith, K. M., Ed.; Elsevier: Amsterdam, 1975.

(46) We have been unable to obtain crystals of $NiTC_5TPP$ suitable for X-ray structural analysis. The low solubility of $NiTC_5TPP$ also presented a problem in verifying the formation of the Ni complex. A dilute carbon disulfide solution of $NiTC_5TPP$ gave a Soret band maximum at 425 nm and a β-band maximum at 520 nm, consistent with a nickel derivative. A more concentrated CS_2 solution of Ni tetracyclopentenyltetra-*p*-tolylporphyrin, prepared in the same manner, gave an absorption spectrum and Raman spectrum similar to that of $NiTC_5TPP$. The $NiTC_5TPP$ peak positions are close to the corresponding bands of NiTPP, NiOEP, and $NiTC_6TPP$, supporting the successful formation of the nickel TC_5TPP derivative. The bands also shift as expected of a nickel porphyrin in coordinating solvents. See Table V.

(47) Medforth, C. J.; Berber, M. D.; Fajer, J.; Smith, K. M.; Barkigia, K. M.; Renner, M. W., unpublished results.

(48) Fajer, J.; Medforth, C. J.; Smith, K. M.; Furenlid, L. R., unpublished results.

(49) Shelnutt, J. A. *J. Phys. Chem.* **1983**, *87*, 605.

Table III. Raman Frequencies (in cm⁻¹) of the Structure-Sensitive Marker Lines and Selected Structural Parameters (Calculated) of Nickel Porphyrins

Ni porphyrin	core size (Å)	$C_\alpha NC_\alpha$ angle (deg)	ν_4 (cm⁻¹)	ν_3 (cm⁻¹)	ν_2 (cm⁻¹)	ν_{19} (cm⁻¹)	ν_{10} (cm⁻¹)	ν_ϕ (cm⁻¹)	Raman data from
NiP	1.938	104.5		1505.5			1649.0		NiP/CH₂Cl₂
NiOEPtriB	1.953	104.5	1383.3	1519.9	1602.7	1603.0	1656.0		NiOEP/CS₂
NiTPP	1.953	104.8	1374.3	1505.0	1571.9	1547.0		1600.5	NiTPP/CS₂
NiTC₅TPP	1.969	105.3		1525.7	1586.5			1599.5	NiTC₅TPP/CS₂
NiTC₆TPP	1.920	105.7	1371.3	1512.9	1576.9	1525.7		1599.9	NiTC₆TPP/CS₂
NiTC₇TPP	1.900	105.7	1368.7	1505.3	1564.1			1598.1	NiTC₇TPP/CS₂
NiOMTPP	1.884	106.0	1362.3	1512.1	1574.3	1520.0		1598.5	NiOMTPP/CS₂
NiOETPP	1.878	106.1	1359.7	1504.7	1562.0	1507		1599.1	NiOETPP/CS₂
NiOPTPP	1.878	106.1	1359.9	1504.5	1559.9	1504		1598.5	NiOPTPP/CS₂
NiDPP	1.896	105.6	1367.3	1510.7	1575.7	1503.0		1600.6	NiDPP/CS₂
			1353.1	1500	1545.1			(1606.2)	
NiOETPP/planar	1.953	104.8							
planar relaxed	2.005	105.1							
NiOEP/triA ethyls	1.956	104.5	1380.4	1520.5		1605.5	1659.0		NiOEP/triA/xtal
NiOEP/triB ethyls	1.953	104.5	1382.9	1524.8		1608.4	1662.2		NiOEP/triB/xtal
NiOEP/tet ethyls	1.953	104.5	1383.0	1514.0		1595.0	1641.0		NiOEP/tet/xtal
NiOEP/alt ethyls	1.952	104.5							
NiTC₅TPP			1392.6	1528.2	1591.0	1566.0		1600.4	NiTC₅TPP/xtals
NiTC₆TPP			1372.6	1512.8	1572.6			1599.4	NiTC₆TPP/xtals
NiTC₇TPP			1368.8	1506.6	1564.4			1598.4	NiTC₇TPP/xtals
NiOETPP			1360.0	1507.0	1565.8			1600.0	NiOETPP/xtals
NiOPTPP			1358.0	1505.6	1559.4			1596.8	NiOPTPP/xtals

Table IV. Calculated Minimum Energies (in kcal/mol) and Some Parameters from the Calculated Structures of the Nickel Octaalkyl(aryl)tetraphenylporphyrins

porphyrin	total energy	torsion energy	VDW energy	angle energy	bond energy	Ni–N distance[a]	$C_\alpha NNC_\alpha$ dihedral[b]	N–Ni–N angle[b]	av ϕ dihedral angles[b]
NiP	86.2	0.0	10.9	71.6	3.7	1.938	0.0	180.0	
NiOEP	120.8	0.4	32.3	77.8	10.3	1.953	0.2	180.0	
NiTPP	242.1	79.3	73.9	74.3	14.4	1.952	0.8	180.0	
NiTC₅TPP	338.1	108.0	66.2	142.0	21.9	1.969	0.1	179.9	89.9
NiTC₆TPP	345.4	127.9	103.6	91.4	21.6	1.935	0.8	165.8	78.8 (81.6, 68.9)
NiTC₇TPP	388.6	142.6	112.8	106.4	25.9	1.920	2.2	163.3	74.3 (88.1, 60.4)
NiOMTPP	324.2	127.3	86.7	90.6	19.0	1.907	3.7	162.0	62.1
NiOETPP	360.2	149.1	87.1	98.7	23.2	1.903	7.8	161.3	70.1
NiOPTPP	370.0	149.3	93.6	99.9	25.0	1.903	8.6	161.5	70.1
NiDPP	535.5	279.6	139.5	82.8	28.9	1.915	1.7	163.8	
NiOETPP/planar	426.9	105.7	169.3	120.0	31.1	1.952	0.8	180.0	
planar relaxed	398.5	120.8	124.4	111.2	41.5	2.005	4.5	179.9	
NiOEP/triA ethyls	122.6	0.3	33.1	78.5	10.8	1.953	0.2	180.0	
NiOEP/triB ethyls	120.8	0.4	32.3	77.8	10.3	1.953	0.2	180.0	
NiOEP/tet ethyls	122.7	0.4	33.1	78.5	10.7	1.953	0.1	179.1	
NiOEP/alt ethyls	119.2	0.5	31.7	77.2	9.9	1.953	0.6	180.0	

[a] Distances in Å. [b] Angles in deg.

lines are given in Table III. The frequency comparisons are not as accurate (roughly ±1 cm⁻¹) as the data obtained by using the dual-channel mode of the Raman spectrometer.

UV–visible absorption spectra of the four-coordinate NiOATPPs were obtained in carbon disulfide and dichloromethane; absorption spectra of the six-coordinate forms were obtained in the coordinating solvents pyrrolidine, piperidine, and pyridine. The UV–visible spectra were taken using a Model 330 UV–visible-NIR spectrophotometer (Perkin-Elmer).

Results

Molecular Mechanics Calculations. The calculated structures of porphyrins 1–6 and 8–10 are shown in Figure 1, and Tables III and IV give some relevant structural parameters obtained from the molecular energy optimization calculations. Among the calculated structures, the core size (δ) varies from 1.878 to 1.969 Å (Table III), while the Ni–N distance shows a similar variation (Table IV). (The core size, δ, is defined in this work as the length of the projection of the metal–nitrogen (M–N) bond into the average plane of the pyrrole nitrogens. When the nitrogens are located in the root-mean-square plane, δ is the center-to-nitrogen (Ct–N) distance. However, for the ruffled structures of the NiOATPPs the nitrogens are generally above or below the mean plane of the nitrogens, and δ is distinct from the Ct–N distance. Core size, defined in this way, is the radius of a cylinder through the porphyrin core with the nitrogens located on the cylindrical surface.) The calculated core size generally gets smaller as the porphyrin ruffles, in agreement with the trend first noted by

Hoard.[50] Ruffling allows (or forces) the core to contact. The degree of the ruffling of the macrocycle is measured by using two parameters which correspond to two distinct modes of ruffling: (1) pyrrole twisting, defined by the dihedral angle between the planes of opposite pyrrole rings or the $C_\alpha N$–NC_α dihedral angle, and (2) pyrrole tilting, defined by the angle between opposite pyrrole nitrogens with Ni at the vertex (N–Ni–N angle in Table IV). The former ruffling gives a saddle structure with axes through opposite bridging carbons; the latter mode of ruffling gives a saddle structure with axes through the pyrrole nitrogens. These two parameters give a rough measure of the two distinct types of macrocycle ruffling that can occur and together give a measure of the degree of nonplanarity. For example, NiOPTPP has the most nonplanar structure of all the nickel porphyrins with a pyrrole twist of almost 9° and a tilt of the pyrroles of 9.25° = (180°−161.5°)/2. The latter pyrrole tilt angle is the angle between the mean plane of the porphyrin and the Ni–N bond and is calculated by using the N–Ni–N angle from Table IV.

Calculated energies for the nickel porphyrin structures are also given in Table IV. The total energy approximately follows the nonplanarity and the size of the β-pyrrole substituents. The increase in the total energy is a result of the increase in van der Waals interactions of the substituents at the periphery of the porphyrin. However, the increase in energy is manifested in a
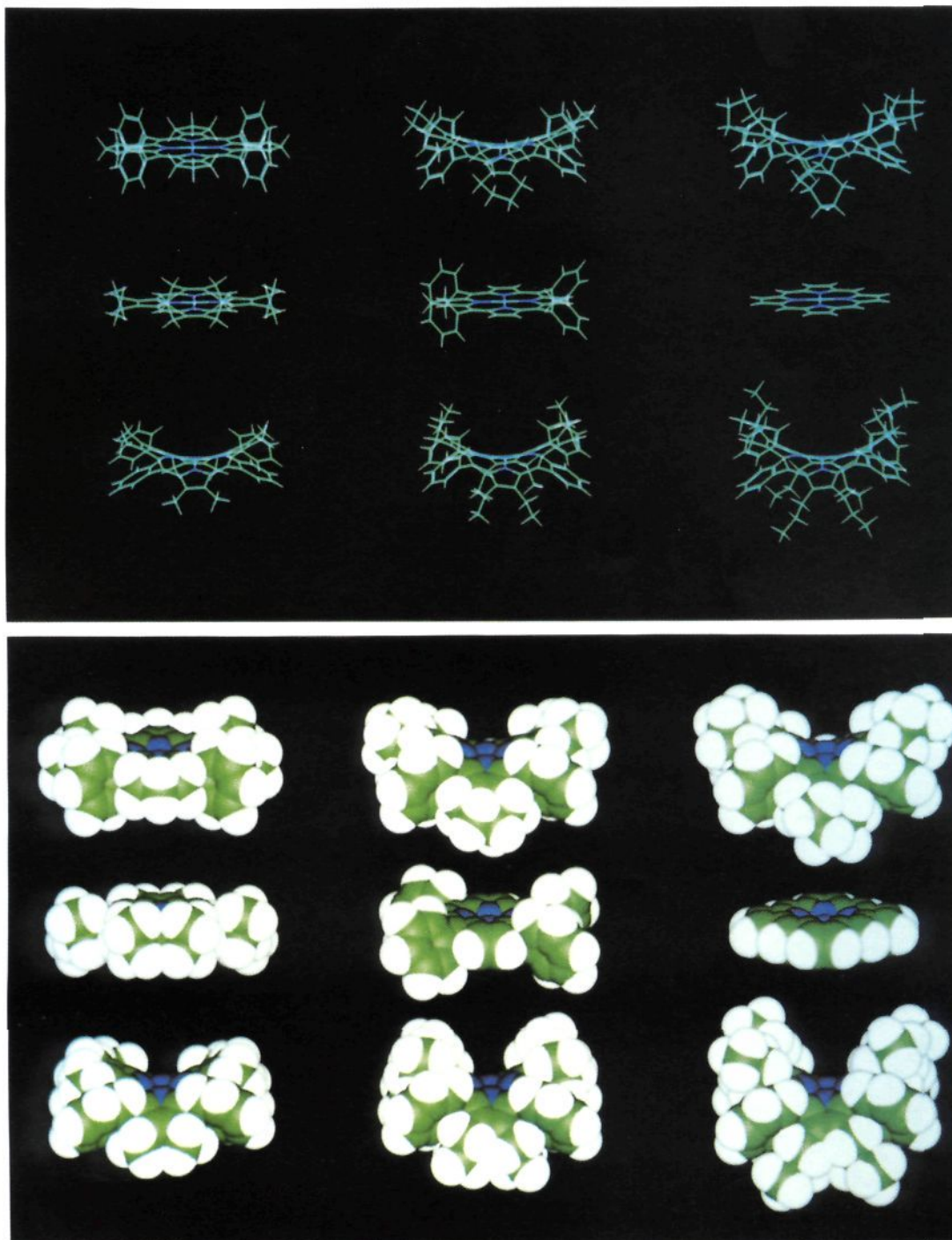
(50) Hoard, J. L. *Ann. N.Y. Acad. Sci.* **1973**, *706*, 18.

Figure 1. Energy-optimized structures of the nickel octaalkyl(aryl)tetraphenylporphyrins (top left to bottom right: **8**, **9**, **10**, **1**, **2**, **3**, **4**, **5**, **6**).

complicated mixture of increases in torsion-, angle-, and bond-strain energies that result from the adjustment of the structure to the mounting van der Waals repulsions as the size of the C_β substituents increase. Nevertheless, the majority of the increase in energy among the structures shows up in the van der Waals energy and the torsions. The torsion force constants primarily act to main the planarity of the macrocycle and, hence, are most affected by nonplanar distortions. Distortion from planarity caused by steric congestion at the periphery of the porphyrin has been observed in the crystal structure of an octaethylmesodimethyl-porphyrin[51] and in other tetrapyrroles.[10]

Ultraviolet–Visible Absorption Spectra. The peak positions of the α (Q(0–0)), β (Q(0–1)), and γ (Soret or B(0–0)) bands are listed in Table V for two noncoordinating solvents (CS$_2$ and

CH$_2$Cl$_2$) and three coordinating solvents (pyrrolidine, piperidine, and pyridine). Carbon disulfide causes a uniform approximately 12-nm red shift in the Soret band relative to dichloromethane for all of the nickel porphyrins. The solvent shifts for the Q bands are about 7 nm. Nevertheless, the Raman spectra show no evidence of axial ligation, exhibiting only small (<1 cm^{-1}) solvent shifts in the structure-sensitive lines. The large red shift for carbon disulfide (dielectric constant, polarity ($E_T(30)$), refractive index, dipole moment; 2.6, 32.6, 1.628, 0.0, respectively) may be due

---

(51) Lay, K.-L.; Buchler, J. W.; Kenny, J. E.; Scheidt, W. R. *Inorg. Chim. Acta* **1986**, *123*, 91.
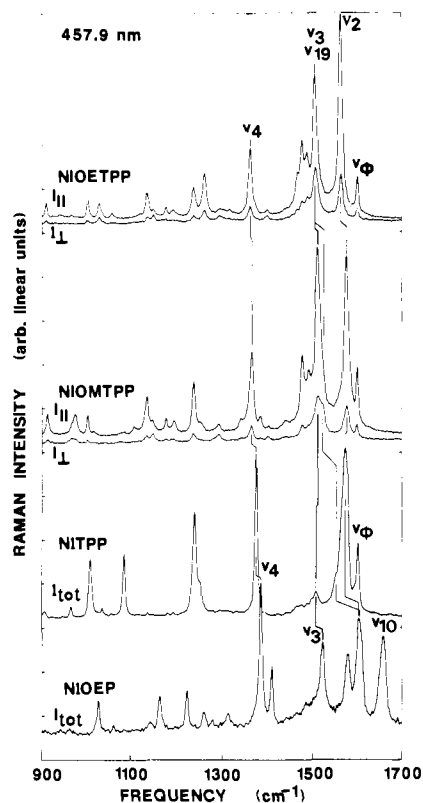
Figure 2. Resonance Raman spectra of NiOETPP ($I_\parallel$ and $I_\perp$), NiOMTPP ($I_\parallel$ and $I_\perp$), NiTPP (I_{tot}), and NiOEP (I_{tot}) in carbon disulfide. Laser excitation was at 457.9 nm. Structure-sensitive marker lines are indicated.

Figure 3. Resonance Raman spectra of NiDPP, NiTC$_7$TPP, NiTC$_6$TPP, and NiTC$_5$TPP in carbon disulfide. Laser excitation was at 457.9 nm except for NiTC$_5$TPP, which was at 413.1 nm.

to either its low dielectric constant, its low polarity, high refractive index, or its lack of a dipole moment in comparison with dichloromethane (8.9, 41.1, 1.424, 5.2).[52] However, the spectra in benzene (2.3, 34.5, 1.501, 0.0), which also has a low dielectric constant and no ground-state dipole do not exhibit a red shift. This suggests that dispersion forces of the solvent (CS$_2$), which are related to polarizability (and the refractive index by the Lorentz–Lorentz equation),[52] give rise to the red shift.

In a given solvent, the wavelengths of the Soret and Q band maxima vary over a wide range for the series of NiOATPPs. For example, the Soret maximum in dichloromethane occurs at 413 nm for NiTC$_5$TPP and at 449 nm for NiDPP. When the whole nickel porphyrin series is considered, the range is from 385 (NiP) to 449 nm (NiDPP) in dichloromethane. The trend is a greater red shift for porphyrins with more extensive and bulky substituents at the periphery (vide infra).

Axial ligation leads to a six-coordinate Ni complex, and when it occurs for nickel porphyrins results in large red shifts (15–20 nm) in the Soret band.[15–18] Even larger red shifts are observed for the α and β bands upon formation of the bis six-coordinate complex. The four-coordinate species, when observed in the coordinating solvents of this study, generally have a Soret band located near the position observed for the Soret in dichloromethane. This is expected because the refractive index for the solvents pyrrolidine, piperidine (1.453), and pyridine (1.510) are generally closer to dichloromethane (1.424) and benzene (1.501) than to carbon disulfide (1.628).[52]

In the case of the NiOATPPs, there is little evidence that even strong bases like pyrrolidine coordinate, because the band maxima occur near the positions found in dichloromethane. The exceptions are NiTC$_5$TPP and possibly NiOMTPP; NiTC$_5$TPP in pyrrolidine exhibits coordination-induced red shifts of the absorption bands.[46] For comparison, NiTPP and NiOEP are almost completely six-coordinate in neat pyrrolidine; nickel tetra(N-methyl-
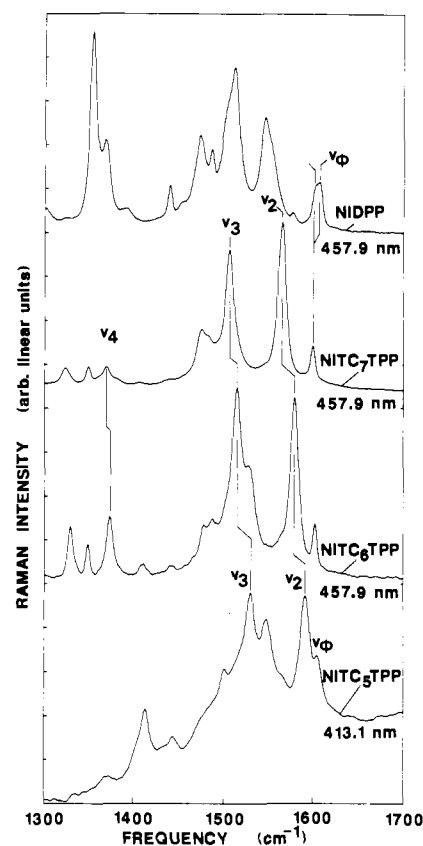
pyridinium)porphyrin even binds weak bases such as water.[53]

Resonance Raman Spectra. Typical resonance Raman spectra of the NiOATPPs in the region between 1300 (or 900) and 1700 cm^{-1} are shown in Figures 2 and 3. This spectral region contains most of the structure-sensitive Raman marker lines, including ν_4, ν_3, ν_2, ν_{19}, and ν_{10}. (The notation and assignments are that of the NiOEP normal coordinate analysis.[38]) The frequencies of these marker lines are listed in Table III. The spectra of the parent NiOEP and NiTPP compounds are also included in Figure 2, and frequencies are listed in Table III for comparison purposes. The spectrum of NiOPTPP is not shown because it is almost identical with that of NiOETPP which is shown in Figure 2.

Many additional strong Raman lines are noted in the NiOATPP spectra, especially in the 1450–1550-cm^{-1} region and below 1300 cm^{-1}, when compared to the parent compounds NiOEP and NiTPP. This is partly a result of the presence of additional Raman lines from both the mesophenyl and C$_\beta$-pyrrole substituents. Also, additional Raman active modes are expected because the symmetry is lowered from D_{4h} by distortion from planarity for most of the porphyrins of the NiOATPP group.

Polarized spectra were obtained to allow us to identify the weak anomalously polarized ($I_\perp/I_\parallel > {}^3/_4$) ν_{19} vibrational mode in many of the spectra. In some cases the position of ν_{19} is surmised from the anomalous depolarization ratio of a degenerate mode near the expected frequency (see Figure 2).

Figure 3 shows the Raman spectra of the series of tetracycloalkenyltetraphenylporphyrins for which the β-pyrrole carbons of each pyrrole are connected by saturated hydrocarbon chains to give five-, six-, and seven-membered rings. The spectrum of NiTC$_5$TPP could not be obtained at 457.9-nm excitation because of low solubility and poor resonance condition. Spectra of the powder were obtained at 457.9 nm, and a CS$_2$ solution spectrum was obtainable near resonance at 413.1 nm. All spectra of

(52) Reichardt, C. *Solvents Effects in Organic Chemistry*; Verlag Chemie: Weinheim, 1979.

(53) Pasternack, R. F.; Francesconi, L.; Raff, D.; Spiro, E. *Inorg. Chem.* **1973**, *12*, 2606.
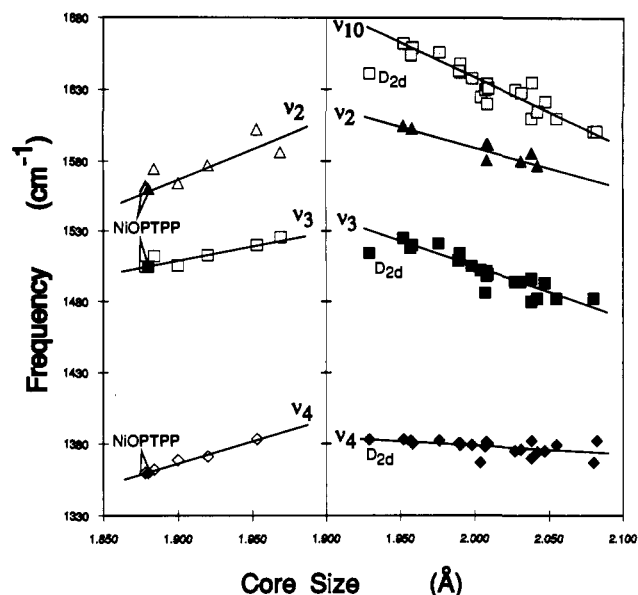
Planar and Nonplanar Nickel(11) Porphyrins

J. Am. Chem. Soc., Vol. 113, No. 11, 1991 4083

Figure 4. Relationship between core size and Raman frequencies for structure-sensitive marker lines ν_4, ν_3, and ν_2 for the NiOATPPs (left panel) and the same Raman lines plus ν_{10} (open boxes) for the MOAPs in Table VI (right panel). The right panel includes data for the NiOEP ruffled (D_{2d}) and planar (D_{4h}) structures. The left panel includes the D_{2d} NiOEP and NiOPTPP X-ray structure data (solid points); the point labeled D_{4h} in the left panel is based on the calculated NiOEP structure.

NiTC$_5$TPP were of significantly poorer quality than for the other porphyrins. The Raman spectrum of NiDPP is also shown in Figure 3.

Figure 4 shows plots of the frequency of three of the structure-sensitive lines, ν_4, ν_3, and ν_2, versus the calculated core size δ. Figure 6 shows a similar plot of the frequencies of these same marker lines versus the C_aNC_a angle. In Figures 4 and 6, the data for the NiOATPPs are superimposed on plots of the Raman data for the many metal octaalkylporphyrins (MOAPs) used in arriving at the well-known correlation with core size for these Raman lines. The MOAPs are generally nearly planar species. The reasons for using the octaalkylporphyrin (OAP) data rather than the tetraphenylporphyrin Raman data in the plots are given in the Discussion section. The core-size marker line data for both the OAPs and the TPPs are listed in Table VI of the supplementary material and were obtained from refs 25–27.

Previous studies of the effects of axial ligation of nitrogenous bases to nickel porphyrins have shown that large shifts occur for the structure-sensitive marker lines.[15-18,54,55] The shifts are partially the result of the larger core size required for the high-spin nickel.[54,55] Raman spectra of NiOETPP in piperidine (not shown) exhibit little evidence of six-coordinate species.

Discussion

Comparison of Calculated Structures and X-ray Crystal Structures. The validity of the spectroscopic correlations with structural parameters relies on the accuracy of the calculated structures. The energy optimization calculations are based on the recently reported structure of NiOEP in the B triclinic form[20] and the reported force consants (Table I, supplementary material) determined from the normal coordinate analysis.[38] Equilibrium bond distances used in the energy minimization calculations were adjusted to match the average bond distances and angles of the triclinic B structure. Therefore, the energy-minimized structure of NiOEP necessarily reproduces the crystal structure accurately. For example, bond distances are reproduced to about 0.005 Å, roughly the uncertainty in the bond distances from the two known *planar* triclinic A[37] and B[20] crystalline forms of NiOEP. The

calculations apparently overestimate the C_aNC_a angle slighty (104.5° versus 104.1° (observed)).

The only other reported nickel–porphyrin structures in the series are those of *ruffled* NiOEP and NiTPP crystalline forms. Only the Ni–N bond distance of 1.928 Å was given for the NiTPP structure,[56] almost the same value as for the NiOEP ruffled form (1.929 Å).[37] The calculated Ni–N distance for NiTPP in a *planar* structure is larger, 1.953 Å, the same as calculated for planar NiOEP. For the force field used, the planar forms of NiOEP and NiTPP are unfortunately the only structures predicted, even though both planar and ruffled forms coexist in solution for NiOEP.[19]

The only true test of the accuracy of the calculations is the recently obtained X-ray crystal structures of NiOPTPP.[39] Two almost identical structures were obtained for different crystalline forms at room temperature and at 200 K. Because the calculations predict this porphyrin of the series to have the most ruffled structure, the calculation of its structure provides the most demanding test of our predictive capability.

Generally, the two NiOPTPP structures are similar to the previously reported structure of zinc OETPP with methanol bound to the metal[43] and to the calculated NiOPTPP structure shown in Figure 1. In particular, the macrocycle is strongly ruffled with the pyrrole rings alternately tilted above and below the mean porphyrin plane. For NiOPTPP, the tilting of the pyrrole rings results in the nitrogens being alternately above and below the mean plane by 0.173–0.199 Å (0.184 to 0.185 Å at room temperature). The calculated structure gives the same general structure, and some twisting of the pyrroles occurs in addition to the pyrrole tilting. The calculated out-of-plane distance of the nitrogens due to pyrrole tilting is 0.306 Å. Thus, the calculation slightly overestimates this measure of the degree of ruffling, nevertheless reproducing the basic nonplanar distortion of the macrocycle.

For the elucidation of the Raman correlations, the nickel core geometry is of vital importance. The average Ni–N distance for the low-temperature structure is 1.902 ± 0.002 Å; the Ni–N distance for the room-temperature structure is the same within experimental uncertainty, 1.899 ± 0.003 Å. The experimental values compare favorably with the calculated Ni–N distance of 1.903 Å. The core size is 1.890 Å, slightly larger than the calculated core size of 1.878 Å. The underestimate of the core size is probably a result of the excessive ruffling predicted by the calculations and suggests that slightly stiffer torsion force constants are necessary to more accurately predict porphyrin structures in the crystal phase. The Ni ion in the X-ray structures is less than 0.02 Å from the average plane of the porphyrin as calculated.

The C_aNC_a angle is also fairly accurately predicted by the energy-minimized structure. The calculated value of 106.1° is to be compared with 105.8 ± 0.1° for the low-temperature structure and 105.7 ± 0.3° for the room-temperature structure. The slight overestimate of the angle is almost identical with the error in calculating the reference NiOEP structure (104.5° calculated versus 104.1° observed). For our purposes, it is the comparison between structures, not the prediction of X-ray structures, that is important.

It is evident that the energy optimization calculations using the NiOEP force field are exceptionally precise in predicting the core geometry even in the most difficult case of NiOPTPP. Thus, we can with some confidence believe the correlations between Raman frequencies and core size or C_aNC_a angle given in Figures 4 and 6, especially since the structures at opposite ends of the series, planar NiOEP and highly ruffled NiOPTPP, are known and were accurately predicted.

The calculated structure of NiTC$_5$TPP is unusual in that it is the only planar structure of all of the NiOATPPs. In an earlier report we investigated the saddle inversion equilibrium for the tetracycloalkenylmesotetraphenylporphyrins.[42] Inversion barriers for TC$_n$TPP free base, dication, and nickel derivatives decrease in the series OETPP > TC$_7$TPP > TC$_6$TPP > TC$_5$TPP. Although

(54) Findsen, E. W.; Shelnutt, J. A.; Ondrias, M. R. *J. Phys. Chem.* **1988**, *92*, 307.

(55) Findsen, E. W.; Alston, K.; Shelnutt, J. A.; Ondrias, M. R. *J. Am. Chem. Soc.* **1986**, *108*, 4009.

(56) (a) Hoard, J. L.; Sayler, A., unpublished results. (b) Scheidt, W. R.; Lee, Y. J. *Structure and Bonding* **1987**, *64*, 1.
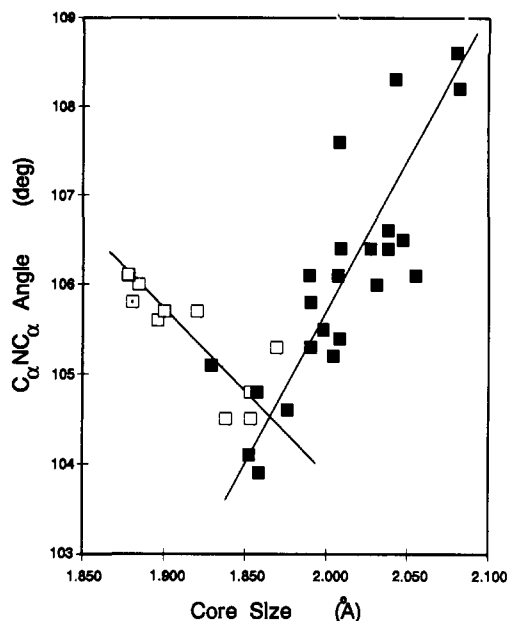
4084 *J. Am. Chem. Soc., Vol. 113, No. 11, 1991*

Shelnutt et al.

Figure 5. Relationship between core size and $C_\alpha NC_\alpha$ angle from X-ray structural data for the OAPs (filled points), from calculated NiOATPP structural data (open points), and from the X-ray structure of NiOPTPP (□ point).
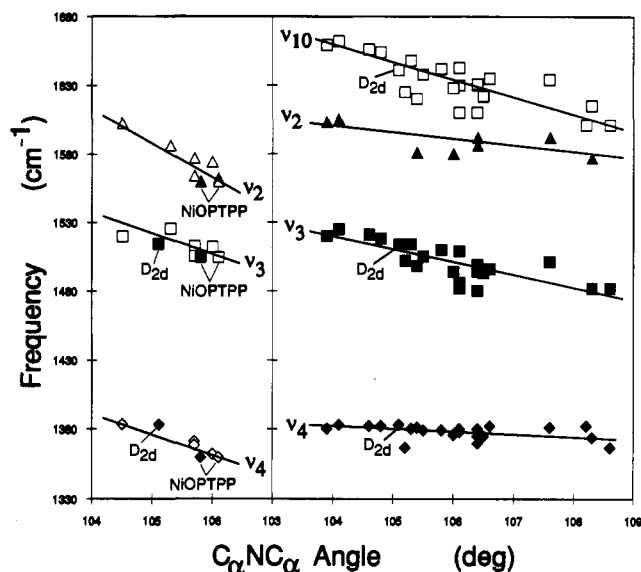

Figure 6. Relationship between $C_\alpha NC_\alpha$ angle and Raman frequencies for structure-sensitive marker lines. Data points are the same as for Figure 4.

poor solubility prevented the measurement of the barrier to inversion for NiTC₅TPP, the trend in ΔG for porphyrin inversion suggests that the barrier vanishes, indicating NiTC₅TPP is essentially planar. The absorption spectral data discussed in the Experimental Section supports a planar structure for NiTC₅TPP, in agreement with the calculated structure. Apparently, steric interaction between the five-membered ring and the phenyl substituents is negligible, resulting in a planar porphyrin. This is certainly the case for the calculated NiTC₅TPP structure, for which the van der Waals interaction (66.2 kcal/mol) is intermediate between unhindered NiOEP (32.3 kcal/mol) and NiTPP (73.9 kcal/mol). The constrained "planar" NiOETPP structures in Tables III and IV represent an attempt to calculate an upper limit for ΔH of the barrier for inversion of NiOETPP. NiOETPP was constrained during minimization into the planar porphyrin-skeleton conformation of NiTPP and then "relaxed". The energy was very sensitive to the orientations of the ethyl substituents. The lowest energy conformation of the ethyl groups for planar NiOETPP and NiOEP (see Table IV) was that in which the ethyls

alternate in pointing above and below the porphyrin plane. When the planar constraint is relaxed for this conformation of the ethyl groups a local minimum in the energy is found for a nearly planar structure. The results for this relaxed planar form are given in Tables III and IV. The difference in total energy for the ruffled and relaxed planar structures (38.3 kcal/mol) is about three times ΔG for inversion for NiOETPP obtained experimentally (13.2 kcal/mol). This planar NiOETPP form has an inordinately expanded porphyrin core (2.005 Å).

There is an apparent effect of metal size on the degree of core contraction that is allowed as a result of substituent-induced ruffling. In contrast with the strong core contraction observed for ruffled NiOPTPP when compared to planar Ni porphyrins, ruffled ZnOETPP shows only a small contraction when compared with a planar Zn porphyrin.[57] The contraction for ZnOETPP is only 0.01 Å relative to the nearly planar Zn(py)TPyP[56] complex (ZnOETPP, 2.036 Å/Zn(py)TPyP, 2.047 Å). The Zn(II) ion is larger than the optimal core size and resists the contraction of the core induced by ruffling. Core contraction is favored by both the small, low-spin Ni(II) ion and substituent-induced ruffling for NiOPTPP, resulting in an approximately 5–6 times larger core contraction (0.06 Å) for nickel than for zinc (NiOPTPP, 1.890 Å and NiOEP triclinic B, 1.952 Å). Thus, larger metals apparently resist the core contraction caused by substituent-induced ruffling. This may explain the ease with which Zn can be removed from the ruffled OATPPs.[43] The size of the metal has a much smaller effect on the increase in the $C_\alpha NC_\alpha$ angle due to substituent-induced ruffling. The substituent-induced increase in the angle due to ruffling is 1.1° for zinc (Zn(MeOH)OETPP, 107.7°/Zn(py)TPyP, 106.6°) and 1.7° for nickel (NiOETPP, 105.8°/NiOEP triclinic B, 104.1°).

Effect of Nonplanarity on Visible Absorption Spectra and Ligand Binding Affinities of Nickel Octaalkyl(aryl)tetraphenylporphyrins. The NiOATPP derivatives show an increase in the wavelength of the π–π* transitions (α, β, and Soret bands) as bulkier groups are substituted at the β-pyrrole positions (Table V). This is apparent especially in the NiTC$_n$TPP (n = 5, 6, 7) series, for which greater interaction with the mesophenyl substituents occurs for the larger cyclohexenyl and cycloheptenyl rings. The growing red shift in the Soret bands of the full series, P < OEP < TPP < TC₅TPP < TC₆TPP < OMTPP < OETPP ≅ OPTPP < TC₇TPP < DPP, can be accounted for, in part, by an increase in the nonplanarity of the porphyrins. Iterative extended Hückel (IEH) molecular orbital calculations have shown that a red shift in both the Soret and Q bands is expected upon ruffling.[19] This prediction has been born out by more rigorous molecular orbital calculations for Ni porphyrins[58] and Zn porphyrins[10] by using the intermediate neglect of differential overlap (INDO) method with configuration interaction (CI). Thus, the increasing red shift alone suggests that the nonplanarity is increasing in the series. This interpretation is further supported by our calculated structures (by using either core size, $C_\alpha NC_\alpha$ angle, NNiN angle, pyrrole twist angle, energy, or root-mean-square distortion from planarity as the measure of nonplanarity within the NiOATPP series).

For the porphine, OEP, TPP, and DPP derivatives, an additional electronic effect might come into play in determining the absorption band positions, because the electron-withdrawing-donating properties of the substituents[59] are significantly different both within this subgroup and between these nickel porphyrins and the NiOATPPs. For instance, DPP has 12 electron-withdrawing phenyl substituents compared with OEPs eight electron-donating ethyl groups. An additional effect is the delocalization of π-charge density onto carbon substituents, which does not occur for hydrogens.[60] This hyperconjugation effect differs for these porphyrins. These electronic effects should have a negligible influence

(57) Collins, D. M.; Hoard, J. L. *J. Am. Chem. Soc.* **1970**, *92*, 3761.
(58) Courtney, S. H.; Jedju, T. M.; Friedman, J. M.; Rothberg, L.; Alden, R. G.; Park, M. S.; Ondrias, M. R. *J. Opt. Soc.*, in press.
(59) (a) Johnson, C. D. *The Hammett Equation*; Cambridge University: London, 1973. (b) Hansch, C.; Leo, A. *Substituent Constants for Correlation Analysis in Chemistry and Biology*; Wiley-Interscience: New York, 1979.
(60) Shelnutt, J. A.; Ortiz, V. *J. Phys. Chem.* **1985**, *89*, 4733.

Table V. Wavelength of Absorption Maxima (in nm) of the Nickel Octaalkyl(aryl)tetraphenylporphyrins in Various Coordinating and Noncoordinating Solvents

	carbon disulfide			dichloromethane			pyrrolidine			piperidine			pyridine		
	γ	β	α	γ	β	α	γ	β	α	γ	β	α	γ	β	α
NiDPP (4-coord)	459	573	623	449	566	613	448	566	608						
(6-coord)															
NiOPTPP (4-coord)	445	560	596	434	553	590	435	553	590						
(6-coord)															
NiOETPP (4-coord)	445	561	594	433	552	585	434	552	589	435	553	590	434	551	590
(6-coord)															
NiOMTPP (4-coord)	441	555	591	429	549	583	437[a]	553[a]	600[a]	438[a]	555[a]	604[a]			
(6-coord)															
NiTC₇TPP (4-coord)	451	563	600	440	556	595	443	559	600						
(6-coord)															
NiTC₆TPP (4-coord)	437	550	586	424	543	579	427	545	582	428	547	583			
(6-coord)															
NiTC₅TPP (4-coord)	425	520		413											
(6-coord)							429	528	559	430					
NiTPP (4-coord)	424	531	562	414	525	557	413	520		414	519		418	529	
(6-coord)							433	564	603	433	561	600	434		
NiOEP (4-coord)	406	522	558	391	515	551				396		552	393	516	552
(6-coord)							420	544	576	419	542	574			
NiP (4-coord)	398	510	543	385	504	536									
(6-coord)							410	537	570	410	535	569			

[a] May be mixture of four- and six-coordinate forms.

within the NiOATPP series of porphyrins, because all of these porphyrins have only carbon substituents with nearly identical electron-donating properties. On the other hand, the strain on the pyrrole ring caused by the smaller cyclic substituents of the TC$_n$TPP series might affect the UV–visible spectrum by distorting the pyrrole rings.

Axial ligation by nickel porphyrins results in a change in spin state of the nickel ion.[61] Binding of a σ-donating axial ligand raises the energy of the doubly occupied d_{z^2} orbital relative to its energy for the unligated nickel porphyrin ($S = 0$), resulting in promotion of one electron to the unoccupied $d_{x^2-y^2}$ orbital and a change in spin ($S = 1$). The change in interaction of the high-spin nickel with the porphyrin ring results in a red shift in the absorption bands. It might be expected that the population of the antibonding $d_{x^2-y^2}$ orbital would, by itself, result in a larger core. And, this is the case as demonstrated by Raman results.[54,55] The metal $4p_z$ orbital's interaction with the ligand and macrocycle may also play a role in determining the red shift in the bands.[62]

Examination of Table V shows that axial coordination does not occur for the significantly ruffled porphyrins of the NiOATPP series. This is surprising in view of the usual electronic influences of substituents upon axial ligand affinity in nickel porphyrins. For Ni porphyrins that exhibit large populations of the planar conformer, axial ligand affinity for bases like piperidine or water depends on the electron-withdrawing properties of the peripheral substituents. For example, the series of porphyrins, NiOEP < NiProtoP < NiTPP < NiTMePyP, shows increasing affinity for σ-donating ligands as the electron-withdrawing properties of the substituents increase. For porphyrins in the NiOATPP series, which have both electron-donating alkyl β-pyrrole substituents and electron-withdrawing mesophenyl substituents, one expects to find ligand affinities intermediate between NiOEP and NiTPP. Actual ligand affinities of the ruffled NiOATPPs are much lower than either NiOEP or NiTPP.

The low axial ligand affinity of the NiOATPPs can be explained in two ways. First, the ligand affinity is expected to be lower for a ruffled nickel porphyrin than for a planar one. The contracted core of a ruffled porphyrin raises the energy of the $d_{x^2-y^2}$ orbital to which an electron must be promoted upon coordination of an axial ligand. Promotion of an electron must occur to leave a half-empty d_{z^2} orbital to accept charge from the lone pair of the coordinating base. The extra energy required to promote an

electron to the raised $d_{x^2-y^2}$ orbital of the ruffled porphyrins lowers the ligand affinity. A second consideration is the steric constraints imposed by the quasi-axial orientation of the pyrrole substituents. Especially for the propyl and ethyl derivatives, steric hindrance of the ligand can impede binding of a bulky ligand. A narrow groove formed by alkyl substituents on opposite pyrroles could severely limit the orientation of an axial ligand, possibly reducing ligand affinity. The plane of the imidazole (Im) rings of the NiTMePyP(Im)$_2$ complex forms an angle of 23° with the Ni–N bond.[63] For NiOPTPP and NiOETPP the steric interactions with the quasi-axial propyl and ethyl substituents may come into play, forcing a smaller angle.

Raman Spectra of Nickel Octaalkyl(aryl)tetraphenylporphyrins. As can be seen in the spectra of Figure 2, the Soret resonance Raman spectra of the NiOATPPs exhibit characteristics of both TPP and OEP. For example, many vibrational lines characteristic of TPP also occur in the spectra of the NiOATPPs, including phenyl group modes like the line (ν_ϕ) at 1599 cm^{-1}. The result is an increase in the number of Raman active modes for the NiOATPPs compared with either NiOEP or NiTPP. Also, some vibrational modes that are weak in the spectra of NiOEP and NiTPP become strong in the NiOATPP spectra. A good example is the complicated region between 1450 and 1550 cm^{-1}. Many strong lines in the region are evident in the spectra of the NiOATPPs. These lines may be present in the spectra of NiOEP and NiTPP, but they are much less prominent. Enhancement of these modes may be a result of the lower symmetry resulting from out-of-plane distortion of the macrocycle; however, we note that they are also prominent in the planar NiTC₅TPP (Figure 3). We also note that ν_{10} of NiOEP, which is absent in NiTPP, is also absent from the spectra of the NiOATPPs. Curiously, two lines between 1300 and 1360 cm^{-1} gain intensity for the cyclic NiTC$_n$TPPs ($n = 5, 6, 7$) but are hardly noticeable in the Raman spectra of the other NiOATPPs.

The assignment of the lines in the spectrum of NiDPP is not clear-cut. But the obvious assignments of the modes give very low frequencies for ν_2 and ν_4. Considering that other (higher frequency) lines could also be assigned to ν_2 and ν_4 and considering the extraordinary widths of many of the lines, it is possible that multiple nonplanar conformers of NiDPP coexist in solution. Previously, planar and nonplanar conformers have been found to coexist in solution for several nickel porphyrins.[19,21,22] Multiple nonplanar conformers of a nickel hydrocorphinate have also been observed in solution.[64]

(61) La Mar, G. N.; Walker, F. A. In *The Porphyrins*, Dolphin, D., Ed.; Academic: New York, 1978; Vol. 4, Chapter 2.

(62) Shelnutt, J. A.; Straub, K. D.; Rentzepis, P. M.; Gouterman, M.; Davidson, E. R. *Biochemistry* **1984**, *23*, 3946.

(63) Kirner, J. F.; Garofalo, J., Jr.; Scheidt, W. R. *Inorg. Nucl. Chem. Lett.* **1975**, *11*, 107.

4086 *J. Am. Chem. Soc., Vol. 113, No. 11, 1991*

Shelnutt et al.

The phenyl mode at about 1600 cm^{-1} is clearly a doublet for NiDPP but a single line for the other NiOATPPs. This phenyl mode shows very little variation in frequency for a large range of mesophenyl porphyrins, including the porphyrins in this study (1598–1601 cm^{-1}). Therefore, it is tempting to assign the lower frequency component of the doublet (at 1600.6 cm^{-1}) to the phenyls at the bridging carbons of the macrocycle and the high-frequency component at 1606.2 cm^{-1} to the phenyls substituted at the pyrrole positions. However, the possible presence of multiple conformers casts some doubt on these assignments.

Although changing the noncoordinating solvent from dichloromethane to carbon disulfide results in a large red shift in the absorption spectrum ($\sim$12 nm, Table V), the solvent change has almost no effect on the Raman spectrum. For example, the structure-sensitive lines of NiOPTPP between 1300 and 1700 cm^{-1} vary by less than 1 cm^{-1} for the two solvents. The lack of solvent Raman shifts, and thus lack of change in the core structure, should be constrasted with the large frequency shifts that accompany axial coordination of two basic ligands, such as pyrrolidine.[15–18,55]

Relationship between Raman Frequencies and Structural Parameters. Figure 4 shows the relationship between core size and the frequencies of ν_4, ν_3, and ν_2. The points with core sizes determined from X-ray crystal structure data are shown with filled boxes, the points with core sizes obtained from calculated structures of the NiOATPPs are shown with open boxes. Clearly, the core-size dependence in the two data sets is different, with the slope being negative for the usual core-size correlation and positive for the correlation exhibited by the new NiOATPP results.

A possible origin for the different correlations is suggested if one notes that the NiOEP ruffled (D_{2d}) structure,[37] which is the most highly nonplanar structure of the original core-size data, lies far off of the linear relationship obeyed by the rest of the original data (especially for ν_3, ν_{19}, and ν_{10}). Further, we now see that the ruffled (D_{2d}) NiOEP structure falls along the correlation for the new NiOATPP data (note data for ν_3 in Figure 4). These observations suggest that the increasing nonplanarity of the series of new structures may account for the difference in frequency dependence versus core size of the NiOATPPs. Indeed, the Raman frequencies correlate with several measures of the degree of nonplanarity of the porphyrin macrocycle, including the core size, NNiN (opposite nitrogens) angle, and root-mean-square deviation from planarity.[42]

Most of the data used in the original core-size correlation[25] is from nearly planar porphyrin complexes. Any structural parameters that happen to correlate with the core size *for planar porphyrins* will necessarily also correlate with the Raman marker line frequencies. For example, Figure 5 shows a plot of the $C_\alpha NC_\alpha$ angle versus the core size for the X-ray crystal structure data used for the original core-size correlation (solid points). The data show a reasonably good correlation between the $C_\alpha NC_\alpha$ angle and core size for these mostly planar porphyrin complexes. Therefore, both structural parameters must correlate with the marker line frequencies. Actually several other angle parameters, including $NC_\alpha C_\beta$, $C_\beta C_\alpha C_m$, and MNC_α, correlate with the frequencies of the structure-sensitive Raman lines, although the correlation coefficient for the $C_\alpha NC_\alpha$ angle is superior.

On the other hand, the NiOATPP data, also included in Figure 5 (open points), show that this correlation breaks down for the nonplanar NiOATPPs and for the ruffled NiOEP structure. This breakdown in the correlation between the two parameters provides an opportunity to discover which parameter is more closely related to the marker line frequencies. As we have already seen, the core size gives distinct correlations for the two data sets, and, hence probably is not the determining factor for the marker line frequencies. However, the $C_\alpha NC_\alpha$ angle is still a candidate and may be related to the Raman frequencies in a similar manner for both data sets.

Again, for the original core-size marker data set, both core size *and $C_\alpha NC_\alpha$ angle* are related, so it is not clear which parameter determines the Raman frequencies. Figure 6 shows the plot of

the frequency of ν_4, ν_3, and ν_2 versus $C_\alpha NC_\alpha$ angle for the original data set and, in addition, for the NiOATPPs. Although the scatter is somewhat greater than for the core-size correlation, it is clear that similar relationships hold for both the original and new data sets. The greater scatter for the angle correlation (rms error = 1.8 versus 1.4 cm^{-1}) for the original data could be due partly to the larger experimental error in determining the angle in the crystal structures. Of course when the combined data set is considered, the angle correlation is better (rms error = 1.6 versus 2.7 cm^{-1}) than for the core-size correlation. The slope for the NiOATPP data appears to be steeper for ν_2 and ν_4 than for the planar porphyrins, but remember that we are comparing the OATPPs with the OAPs, so a slightly different relationship is expected. Also, large angle data points to be obtained for ruffled porphyrins containing metals larger than Ni may lower the slopes considerably. On the other hand, it would be useful if changes in core size caused by differing modes of macrocycle distortion (e.g., ruffling and metal substitution) do result in different core-size (or angle) versus frequency relationships. Then, different patterns of frequency shifts could be identified with a particular type of distortion of the porphyrin ring.

One may wonder why the OAP Raman data is plotted in Figures 4 and 5 rather than the TPP data. One reason is that the scatter in the correlations for the metal TPPs is greater than for the metal OAPs. The more significant reason is that the linear relationship is shifted to lower frequency for the TPPs relative to the OAPs, and the slopes are somewhat different. The TPP shift appears not to occur for the OATPPs. The Raman frequencies of planar NiTC$_5$TPP should establish the relative positions of the OATPPs relative to planar porphyrins like those used in the original core-size correlation studies. However, the frequencies for NiTC$_5$TPP actually fall near or above the OEP data, not below as might have been expected based on the TPP correlations. Hence, we consider the OAP–OATPP comparison to be the most valid.

A curious feature of the core-size correlation has been that these normal modes involve the C_m–C_α stretching motion, a vibration that is far removed from the metal center. It was presumed that core expansion affected the C_α–C_m–C_α bridge, thereby influencing modes that contain contributions from C_m–C_α stretching. Unfortunately, no correlation between Raman frequencies and either C_m–C_α bond distance or $C_\alpha C_m C_\alpha$ angle is observed. An equally consistent rationale can be imagined based on the $C_\alpha NC_\alpha$ angle. C_m–C_α stretching and modulation of the $C_\alpha NC_\alpha$ angle are generally coupled motions.

It has been previously noted that extreme distortions of the metal core, either contraction for small metals (Ni) or expansion for large metals (SnCl$_2$), causes significant adjustments primarily in the M–N bond length and in the $C_\alpha NC_\alpha$ bond angle, while essentially preserving the critical N–C_α and C_m–C_α bond lengths.[65] Nevertheless, distortions in the relatively softer $C_\alpha NC_\alpha$ bond angle apparently affect the force constants of the stiffer bonds, resulting in the observed frequency dependence.

Conclusions

As we have seen, the OATPPs provide a unique series of constrained porphyrins varying in the degree of out-of-plane distortion. The series provides a unique opportunity to investigate the effects of out-of-plane distortions on the chemical and physical properties of porphyrins. Ruffling of the macrocycle in the series varies the Ni–N bond distance over a range of 0.066 Å for four-coordinate species. When changes in either oxidation state (Ni(II) to Ni(I))[11] or coordination number[20,37,63] of the nickel are considered, the Ni–N bond can vary over a range of 0.11 Å for nickel porphyrins. Large changes in metal–porphyrin bonding are possible for even the most ruffled members of the NiOATPP series, but the energetics of these changes are modified by the degree of stabilization of the nonplanar conformation (and small core size) by peripheral substitution (or macrocycle saturation

(64) Shelnutt, J. A. *J. Phys. Chem.* **1989**, *93*, 6283.

(65) Collins, D. M.; Scheidt, W. R.; Hoard, J. L. *J. Am. Chem. Soc.* **1972**, *94*, 6689.

for reduced porphyrin derivatives). Such considerations are important from the standpoint of the methylreductase functional mechanism, especially in regards to the relative stabilities of $Ni^{II}P$ radical anion and $Ni^{I}P$ reduced species. The low affinity for axial ligands of the more nonplanar members of the series can be rationalized on the basis of electronic changes caused by ruffling-induced core contraction.

How are shifts in the structure-sensitive marker lines to be interpreted? First, if it is known that out-of-plane distortion does not occur, then we can still use the Raman line frequencies as an indication of core size. However, in the general case in which no a priori knowledge of the structure is available we are in a quandary. For example, a decrease in frequency in the marker lines can be interpreted as either a decrease or an increase in core size depending upon the type of macrocycle distortion. In the unlikely event that the pyrrole angle is the sole determining factor for the frequencies of all of the markers, then only the angle can be determined from the frequencies. No further information about the detailed conformation of the macrocycle that led to the particular $C_\alpha NC_\alpha$ angle is available in this case. If, however, different modes of distortion lead to somewhat different relative slopes for the angle-frequency correlations, then it may be possible to obtain more information about the various modes of distortion of the macrocycle. Further studies of this class of porphyrins, for which the conformation of the macrocycle can be modified in a known way, would be useful in amplifying the proper mode of usage of the structure-sensitive Raman markers.

Additional Raman studies exploiting the unique structural properties of this series of porphyrins are being undertaken. For example, studies of axial ligation to nickel OATPPs are in progress to fully elucidate the effect of planarity on ligand affinity. Also, metal effects on the OATPP series are being investigated. And, we are investigating the effects of substituent-constrained ruffling on the d–d excited state in the series of nickel porphyrins by using

a new dual-channel transient Raman spectrometer.[22] Finally, we are investigating the possibility of multiple conformations[21,64] of the NiOATPPs in solution, a distinct possibility in the case of NiDPP.[66]

Note Added in Proof. Furenlid et al. (Furenlid, L. R.; Renner, M. W.; Fajer, J., private communication) have determined the Ni–N distances in powder samples of $NiTC_5TPP$ and NiOPTPP. They are 1.99 and 1.92 (±0.02) Å, respectively. The latter value agrees with the crystallographic results (1.902 Å), within experimental error. The distances in $NiTC_5TPP$ are characteristic of a planar macrocycle, as deduced in the text.

Supplementary Material Available: Tables I and II give the force field parameters used in the molecular structure calculations, Table I gives the bond, angle, torsion, and inversion force constants, Table II gives the parameters of the nonbonding potential energy functions, and Table VI lists the Raman frequencies and X-ray structural data for metal octaalkylporphyrin and tetraphenylporphyrin core-size correlations (2 pages). Ordering information is given on any current masthead page.

(66) Sparks, L. D.; Medforth, C. J.; Smith, K. M.; Shelnutt, J. A., unpublished results.

FTIR Evidence of an Altered Chromophore–Protein Interaction in the Artificial Visual Pigment *cis*-5,6-Dihydroisorhodopsin and Its Photoproducts BSI, Lumirhodopsin, and Metarhodopsin-I

Ulrich M. Ganter,[†] Toru Kashima,[‡] Mordechai Sheves,[‡] and Friedrich Siebert*,[†,§]

Contribution from the Institut für Biophysik und Strahlenbiologie, Albert–Ludwigs-Universität Freiburg, Albertstrasse 23, D-7800 Freiburg, FRG, Department of Organic Chemistry, The Weizmann Institute of Science, 76100 Rehovot, Israel, and Max-Planck-Institut für Biophysik, Kennedyallee 70, D-6000 Frankfurt am Main 70, FRG. Received May 14, 1990

Abstract: FTIR studies of the BSI photoproduct and of the later intermediates lumirhodopsin and metarhodopsin-I of 5,6-dihydroisorhodopsin are reported on. Evidence is presented that in the BSI intermediate the retinal chromophore adopts a relaxed conformation in contrast to the bathorhodopsin intermediate of native rhodopsin. Whereas for the modified pigment, the Schiff base C=N stretching mode and its deuteration-induced isotopic shifts are similar to those of unmodified isorhodopsin, the corresponding values of the photoproducts differ. In addition, alterations in the carbonyl spectral range are observed (protonated carboxyl groups and amide-I). This shows that the chromophore–protein interaction is influenced by this modification. Some molecular events of the thermal decay of the bleached pigment occur at lower temperatures or even at an earlier intermediate of the photoreaction than in native rhodopsin.

Introduction

The vertebrate visual pigment rhodopsin consists of an 11-*cis*-retinal chromophore, **1**,[1] bound via a protonated Schiff base

to the ε-amino group of lysine 296 in the protein opsin. Absorption of light by rhodopsin leads to a series of photoproducts that can be trapped at low temperatures.[1,2] Bathorhodopsin (BATHO) is the first transient species to be trapped at 77 K. Considerable interest has been devoted to BATHO since it was shown that it

---

† Institut für Biophysik und Strahlenbiologie.
‡ The Weizmann Institute of Science.
§ Max-Planck-Institut für Biophysik.
⊥ Abbreviations: BATHO, bathorhodopsin; BSI, blue-shifted intermediate of *cis*-5,6-dihydroisorhodopsin obtained at 80 K; 5,6-diH, *cis*-5,6-dihydro; FTIR, Fourier transform infrared; HOOP, hydrogen-out-of-plane; ISORHO, isorhodopsin; LUMI, lumirhodopsin; META-1, metarhodopsin-1.

(1) *Methods in Enzymology*; Packer, L., Ed.; Academic Press: New York, 1982; Vol. 81.
(2) Ottolenghi, M.; Sheves, M. In *Primary Processes in Photobiology*; Kobayashi, T., Ed.; Springer-Verlag: Berlin, 1987; pp 144–153.